Received: 12 August 2022 | Revised: 4 March 2024 | Accepted: 11 March 2024

DOI: 10.1002/joc.8443

RESEARCH ARTICLE

International Journal of Climatology | RMetS

Precipitation over northern South America and the far-eastern Pacific during ENSO: Phase synchronization at inter-annual time scales

Hernán D. Salas[1] | **Alejandro Builes-Jaramillo**[2] | **Niklas Boers**[3,4,5] | **Germán Poveda**[6] | **Óscar J. Mesa**[6] | **Jürgen Kurths**[4,7]

[1]Facultad de Ciencias Exactas y Aplicadas, Instituto Tecnológico Metropolitano, Medellín, Colombia

[2]Facultad de Arquitectura e Ingeniería, Institución Universitaria Colegio Mayor de Antioquia, Medellín, Colombia

[3]Earth System Modelling, School of Engineering and Design, Technical University of Munich, Munich, Germany

[4]Potsdam Institute for Climate Impact Research (PIK), Potsdam, Germany

[5]Department of Mathematics and Global Systems Institute, University of Exeter, Exeter, UK

[6]Departamento de Geociencias y Medio Ambiente, Universidad Nacional de Colombia, Medellín, Colombia

[7]Department of Physics, Humboldt University, Berlin, Germany

Correspondence
Hernán D. Salas, Facultad de Ciencias Exactas y Aplicadas, Instituto Tecnológico Metropolitano, Medellín, Colombia.
Email: hernansalas@itm.edu.co

Present address
Hernán D. Salas, Facultad de Ciencias Exactas y Aplicadas, Instituto Tecnológico Metropolitano, Medellín, Colombia.

Funding information
Instituto Tecnológico Metropolitano; Institución Universitaria Colegio Mayor de Antioquia; Humboldt University of Berlin; COLCIENCIAS

[Correction added on 9 April 2024, after first online publication: The linking of affiliation of Jürgen Kurths was changed from '3,7' to '4,7' in this version.]

Abstract

We investigated the influence of the El Niño-Southern Oscillation (ENSO) on inter-annual precipitation variability in the far-eastern Pacific (FEP) and northern South America (NSA) using an approach based on phase synchronization (PS). First, we carried out a detailed analysis of observational data to define the inter-annual variability, eliminate the seasonal residual frequencies in hydro-climatic anomalies, and assess the statistical significance of PS. Additionally, we characterized the seasonality of regional patterns of sea surface temperature, surface pressure levels, low-level winds and precipitation anomalies associated with the ENSO states. We found that the positive (negative) precipitation anomalies experienced in the FEP and NSA differ from those previously reported in the literature. In particular, the Guianas (northeastern Amazon) and the Caribbean constitute two regions with negative (positive) rainfall anomalies during El Niño (La Niña), separated by a zone of non-significant anomalies along the Orinoco Low-level Jet corridor. Moreover, we showed that the ENSO signal is phase-locked with inter-annual rainfall and low-level wind variability in most of the study regions. Furthermore, we found consistency in the PS between the Central and Eastern Pacific El Niño indices and hydroclimatic anomalies over the Pacific. However, some areas exhibited PS, although they did not show significant precipitation anomalies, suggesting that the influence of ENSO on tropical climatology manifests not only in terms

Abbreviations: CAR, Caribbean region; EEMD, ensemble empirical mode decomposition; EN, El Niño; ENSO, El Niño—Southern Oscillation; FEP, Far-eastern Pacific; GUI, Guianas region; LN, La Niña; NSA, Northern South America; PS, phase synchronization.

Hernán D. Salas and Alejandro Builes-Jaramillo contributed equally to this study.

of the magnitude of anomalies but also in terms of the phases only. Our approach advances the understanding of climatic anomalies in tropical regions and provides new insights into the non-linear interactions between ENSO and hydroclimatic processes in tropical Americas.

KEYWORDS

ensemble empirical mode decomposition, inter-annual variability, phase-locking, synchronization, tropical rainfall

1 | INTRODUCTION

El Niño—Southern Oscillation (ENSO) is one of the main drivers of Earth's climate at inter-annual time scales. It is composed of *El Niño* (EN, oceanic component) and the *Southern Oscillation* (SO, atmospheric component). EN refers to the warm anomalous sea surface temperature (SST) of the central and eastern tropical Pacific Ocean, which produces a deepening of the oceanic's thermocline, concomitant with the weakening and (sometimes) reversal of the trade winds and displacement of the core of convection from the western to the central and eastern regions of the tropical Pacific. The SO is a stationary wave that produces an atmospheric pressure see-saw between the western and eastern equatorial Pacific (Bjerknes, 1969; Philander, 1983; Sarachik & Cane, 2010). Canonically, ENSO presents two states known as EN and La Niña (LN), which are associated with warm and cool SST anomalies over the central tropical Pacific Ocean, respectively (Chen et al., 2019; Timmermann et al., 2018). Several studies have shown that ENSO states are related to severe hydroclimatic events with important socioeconomic, environmental and ecological impacts around the world (Cai et al., 2020; McPhaden et al., 2010). Both, warm or cold ENSO events may have flavours, like the mild warm and strong cold events in the Central Pacific (CP) or strong warm events in the Eastern Pacific (EP) related to diverse precipitation anomalies around the globe (Freund et al., 2019; Geng et al., 2022; Takahashi et al., 2011).

Northern South America (NSA) experiences hydrometeorological anomalies induced by the perturbations in the tropical Pacific SST, the Walker circulation and Rossby wave-train atmospheric circulation (Cai et al., 2020; Rojo & Mesa, 2020; Wang et al., 2021). During EN (LN), NSA experiences a decrease (increase) in precipitation while the far-eastern Pacific (FEP) Ocean experiences an increase (decrease) in precipitation (Glantz & Ramirez, 2020), NSA experiences higher anomalies over the west coasts of Ecuador and Peru (floodings), and lower precipitation anomalies in Colombia (droughts), which in turn are opposite during LN (Capotondi et al., 2015; Mason & Goddard, 2001; Ropelewski & Halpert, 1987; Sanabria et al., 2018; Takahashi & Martínez, 2019), EP EN events are related to a southward shift of the Intertropical Convergence Zone (ITCZ), which in turn favours intense rainfall in the eastern Pacific, while during CP, dryer conditions prevail in Ecuador and Peru (Cai et al., 2020; Capotondi et al., 2015; Sulca et al., 2018).

Wiedermann et al. (2021) found that for EP EN events there is a reduction of precipitation over NSA while there is no evidence of alterations during CP EN. For LN, there is increased precipitation for both, EP and CP events. Furthermore, the Walker circulation anomalies during ENSO are linked with the anomalous wet/dry conditions over the Amazon basin (Kousky et al., 1984; Marengo & Hastenrath, 1993; Neelin & Su, 2005; Yoon & Zeng, 2010), during EN (LN) subsidence (ascend) branches are situated over the Amazon basin (Friedman et al., 2021; Panisset et al., 2018; Satyamurty et al., 2013). Moreover, the recent studies by Sulca (2021) and Builes-Jaramillo et al. (2023) propose that Walker circulation changes during CP, EP and ENSO fast transitions may induce precipitation and moisture transport anomalies contrasting with canonical ENSO events.

The hydroclimatic variability of NSA and FEP is influenced by a suite of quasi-periodic processes acting on a wide range of diurnal to multi-decadal timescales, with ENSO being the most important at the inter-annual timescales (Arias et al., 2021; Glantz & Ramirez, 2020; Poveda et al., 2011; Rasmussen & Wallace, 1983; Shimizu et al., 2017; Tedeschi & Collins, 2016). In addition, there is a large body of literature on the changes associated with ENSO on climatic features, such as the low-level jets (LLJ) of the NSA. For example, (i) the Caribbean LLJ (CLLJ) has a different relationship with ENSO during its active seasons (JJA and DJF). During DJF, a weak (strong) easterly CLLJ corresponds to warm (cold) SST anomalies in the tropical eastern and central Pacific, whereas in JJA, a strong (weak) easterly CLLJ is associated with warm (cold) SST anomalies in the tropical Pacific (Wang, 2007); (ii) The ChocoJet, which is active during SON, is associated with an reduction (increase) in precipitation over western Colombia during EN (LN) (Poveda & Mesa, 2000; Yepes et al., 2019) and (iii) The Orinoco LLJ (OLLJ), which is active during DJF and during EN (LN), the mean wind vertical profiles (and the intensity of the diurnal cycle) decreased (increased) up to 24% (15%) (Builes-Jaramillo et al., 2022a, 2022b). Although there have been advances in our understanding of the relationships between ENSO and precipitation in the NSA and FEP, questions remain and we are still far from a robust understanding of the impacts, inter-basin climate interactions and possible consequences in the context of climate change (Cai et al., 2020).

Pikovsky et al. (2001) define *synchronization* as an *adjustment of rhythms of oscillating objects due to their weak interaction*. Diverse types of synchronization are known, such as frequency synchronization (FS), phase synchronization (PS), identical synchronization (IS), generalized synchronization (GS) and lag synchronization (LS) (Brown & Kocarev, 2000). In particular, PS implies FS but FS does not imply PS. In addition, the PS approach does not include either the interrelation between the amplitudes or control mechanisms, such as amplitude modulation (AM); however, adequate characterization, quantification, and explanation of the phases are valuable even if the amplitude interrelations are not well known (von Storch et al., 1995). Moreover, the existence of a phase relation implies the possibility to predict the phases of precipitation at inter-annual timescales through ENSO (Schiff et al., 1996). In the last decades, synchronization between ENSO and other processes on different temporal scales has been intensively studied (e.g., annual cycle, low-level jets, Hadley and Walker cells, and Inter-tropical Convergence Zone or ITZC) over the tropical Pacific Ocean (Díaz & Villegas, 2022; Jajcay et al., 2018; Maraun & Kurths, 2005; Mokhov et al., 2011; Salas et al., 2020; Singh et al., 2020; Stein et al., 2011, 2014; Yang et al., 2023; Yun et al., 2021). This will allow improvements in the diagnosis, understanding, and management of water resources for socioeconomic, environmental and ecological purposes.

For NSA and FEP, previous studies have demonstrated the impacts of ENSO on their hydro-climatic variability at interannual timescales using linear and non-linear approaches (Andreoli & Kayano, 2005; Bedoya-Soto et al., 2019; Grimm & Tedeschi, 2009; Poveda et al., 2011, 2020; Takahashi & Martínez, 2019; Waylen & Poveda, 2002; Yoon & Zeng, 2010). However, very few studies have investigated these relationships using synchronization approaches. Salas et al. (2020) investigated GS between the ENSO signal and hydro-climatic variables in Colombia as well as GS between the moisture transported by low-level jets and precipitation at inter-annual time scales. This work sheds light on the GS features between precipitation and the canonical states of ENSO (LN and EN) over Colombia but does not include the regional context and seasonal characterization of such GS patterns. Furthermore, Díaz and Villegas (2022) use wavelet coherence to study the impacts of EN on the reduction of water supply in Colombia, and they found coherence between ENSO indices and precipitation during ENSO events that had a high impact on the reduction of water supply in the country, but they also found discrepancies in the phase differences of the climatic variables analysed. Moreover, Yun et al. (2021) studied whether interannual SST anomalies can also cause synchronized spatial shifts of Hadley and Walker circulations. They found that these two circulations exhibit a phase-synchronized spatial shift only during EN events (not during LN), which coincide with a cross-equatorial northwesterly low-level flow that diverges from an area of anomalous drying in the western North Pacific and converges towards a region with anomalous moistening in the southern central Pacific.

The purpose of this study is: (i) to characterize the seasonal regional patterns of hydro-climatic anomalies in the NSA and FEP during LN and EN, (ii) to provide evidence of PS between the ENSO signal in the tropical Pacific Ocean and the inter-annual variability of rainfall in the NSA and FEP; (iii) to investigate the Phase Difference between the ENSO signal in the tropical Pacific Ocean and rainfall over the NSA and FEP during both states of ENSO, (iv) to quantify the PS between Low-level jet winds and precipitation during ENSO and (v) to study the PS between precipitation and the CP and EP indices of ENSO.

2 | REGION OF STUDY

The region of study is defined by the coordinates 180° W–30° W; 10° S–20° N, which includes the Niño 3.4 region (170° W–120° W; 5° S–5° N) over the tropical Pacific Ocean. Over continental territory, the region of study includes Central America and northern South America (Figure 1). We focus our interest on various zones: (i) the Caribbean region (CAR), which covers the Caribbean Sea and the northernmost part of continental Colombia (80° W–65° W; 5° N–18° N); (ii) the Guianas region (GUI), which is located over the Guianas region and the northeastern Amazon river basin and the easternmost part of the Orinoco river basin (65° W–50° W; 8° S–5° N); (iii) the far-eastern Pacific (FEP) (105° W–80° W and 5° S–5° N) (Jauregui & Takahashi, 2018; Takahashi & Martínez, 2019). Moreover, we analyse PS over the zones associated with the three Low-level jets:(i) The

FIGURE 1 Region of study: (cyan box) the Niño 3.4 region, (dashed black line) Far-eastern Pacific (FEP) zone, (black box) the Caribbean region or CAR, (magenta box) the Guianas region or GUI, (blue boxes) zones associated with low-level jets. [Colour figure can be viewed at wileyonlinelibrary.com]

Caribbean LLJ (CLLJ) (12.5–17.5° N, 80–70° W) (Wang, 2007); (ii) The Choco LLJ (ChocoJet) (2–8° N, 82–77.5° W) (Mejía et al., 2021; Poveda & Mesa, 2000; Yepes et al., 2019) and (iii) The Orinoco LLJ (OLLJ) (6–10° N, 70–65° W) (Builes-Jaramillo et al., 2022a, 2022b; Jiménez-Sánchez et al., 2020).

3 | DATA SETS

3.1 | ENSO indices

To analyse the canonical ENSO, we use the Oceanic Niño Index (ONI), which is used by the US Climate Prediction Center to identify EN (LN) events based on the requirement of sea surface temperature for at least five running three-month seasons to an average above +0.5°C (below −0.5°C) in the central Pacific (the Niño 3.4 region) (Kousky & Higgins, 2007).

To study the different types of EN, we use the three indices proposed by Sullivan et al. (2016) to represent the Central Pacific (CP) EN, Eastern Pacific (EP) EN and Mixed-type EN. They are based on the SST in the Niño 3 and Niño 4 regions, which are the areas with maximum SST warm anomalies of the CP and EP EN, and are defined as (i) CP = Niño4normalized—0.5 * Niño3normalized; (ii) EP = Niño3normalized—0.5 * Niño4normalized and (iii) Mixed-type = EP + CP $\simeq$ Niño3.4normalized, where Niño3normalized, Niño4normalized and Niño3.4normalized denote normalized SSTs anomalies in the Niño3 (5° S–5° N, 150° W–90° W), Niño4 (5° S–5° N, 160° W–150° W), and Niño3.4 (5° S–5° N, 170° W–120° W) regions, respectively (Sullivan et al., 2016).

3.2 | Atmospheric reanalysis ERA5

We use data from the ERA5 atmospheric reanalysis (Hersbach et al., 2019), which provides estimates of atmospheric, land, oceanic, and climatic variables. The ERA5 data cover the Earth on a 30 km grid and it resolves the atmosphere using 137 levels, from the surface up to a height of 80 km. In this work, we use the following variables at monthly resolution: monthly sea level pressure, surface level pressure (over the continent), sea surface temperature as well as zonal and meridional wind speeds at 925 hPa and 850 hPa. These data sets are used over the area 120° E–0° W; 30° S–40° N (available at https://cds.climate.copernicus.eu/cdsapp#!/dataset/reanalysis-era5-single-levels-monthly-means).

3.3 | Global precipitation climatology project

The global precipitation climatology project (GPCP) monthly analysis consists of a merger of various satellite-based estimates over both ocean and land, combined with precipitation gauge analyses over land from the global precipitation climatology centre (GPCC). Satellite-based estimates are a combination of passive microwave estimates over the ocean, passive microwave estimates over land, and estimates from IR or microwave sounders, contributing to higher latitudes. The GPCP offers a homogeneous monthly precipitation product, a 2.5° global grid that spans from 1979 to the present (Adler et al., 2018; Huffman et al., 1997). Data are available on the website https://psl.noaa.gov/data/gridded/data.gpcp.html (accessed 21 February 2022).

3.4 | CPC merged analysis of precipitation

The CPC merged analysis of precipitation (CMAP) provides monthly averaged precipitation rate values obtained from five types of satellite estimates (GPI, OPI, SSM/I scattering, SSM/I emission and MSU) and gauge data. This dataset has two files: (i) precipitation estimates that only include satellite estimates and gauge data, and (ii) an enhanced file that also includes blended NCEP/NCAR Reanalysis Precipitation values. CMAP data are on a $2.5 \times 2.5°$ latitude/longitude grid and span from 1979 to the present (Xie & Arkin, 1997). It is important to clarify that these data are comparable (but should not be confused with) to similar combined analyses by Huffman et al. (1997). Data are available on the website https://psl.noaa.gov/data/gridded/data.cmap.html (accessed 21 February 2022).

4 | METHODS

4.1 | Decomposition method

Diverse techniques exist for decomposing time series into elementary patterns of behaviour, such as trends, oscillations and noise (Ghil et al., 2002). The empirical mode decomposition (EMD) method has become a common and powerful tool for geophysical time-series analysis (Huang et al., 1998; Huang & Wu, 2008; Wu et al., 2008). EMD is useful for decomposing a nonlinear and nonstationary time series into a set of Intrinsic Mode Functions (IMFs), which are extracted through an iterative, adaptive and temporally local procedure that does not force the data to prescribed waves as traditional decomposition methods (e.g., sinusoidal waves or wavelets) (Ghil et al., 2002). However, the EMD method has a shortcoming, as it is often not straightforward to associate physical variability modes with IMFs because each IMF contains information in different frequency bands (Rato et al., 2008; Wu et al., 2008). To address this 'mode mixing' problem, Wu and Huang (2009) proposed EEMD, which allows the decomposition of the original time series into a set of IMFs exhibiting scale-consistent oscillation features. The work of Salas et al. (2022) includes a brief summary of EMD and EEMD methods.

In this work, we use the EEMD method that is an alternative approach to define climate anomalies based on the so-called modulated annual cycle (MAC) (Wu et al., 2008). For the scope of this work, we are interested only in studying low-frequency bands whose periods are above seasonal and annual variability. Then, we use EEMD to remove all variability associated with the intra-annual and seasonal time scales to exclusively analyse the inter-annual variability with periods higher than 1 year.

Finally, we use the statistical test proposed by Ahdesmäki et al. (2005) as a robust method for detecting periodicities in a time series. This method is a rank-based, non-parametric spectral estimator that extends the approach by Pearson et al. (2003) and it is almost insensitive to errors and inconsistencies in the data, such as outliers, missing values, short time series and non-linear distortions. Hence, we use this method to guarantee that after decomposing the climatic time series into different frequency bands using EEMD, the decomposed signal has no significant seasonal, intra-annual, or high-frequency residual variability. Moreover, we include the 95% confidence intervals to test that peaks in the periodograms are distinct from the null hypothesis of a red-noise (Liu et al., 2012). To this end, we compute the periodogram for 1000 independent realizations of a red noise based on an AR(1) stochastic process and then, we take the set of periodogram computations and quantify the 95th quantile, which provides the critical values for the periodogram calculated from observed data. If the periodogram of the data is greater than the critical value at a particular frequency, then the spectrum is said to be statistically different from red noise at a significance level of 0.05 (Matyasovszky, 2013). These procedures are important because nonlinear techniques can be biased by the presence of seasonal residual frequencies in the anomalies (Lange et al., 2018; Salas et al., 2020).

4.2 | Composite analysis

We use a composite analysis method to study the relationships between climatic variables (surface pressures, zonal and meridional wind speeds, surface temperatures and precipitation) during the ENSO states (Boschat et al., 2016; Terray et al., 2003; Xie et al., 2017). The procedure can be summarized as follows: (i) we define the EN and LN states using the ONI index; (ii) we isolate the climatic variables for events previously defined, which constitute the key times; (iii) we isolate the climatic variables and compute the average for all key times and (iv) we use the Terray test (Terray et al., 2003) to verify whether there is a significant difference between the average for the states of ENSO and the Neutral conditions.

4.3 | Phase synchronization

Phase synchronization is a phenomenon in which two or more oscillating systems become coupled and their phases align over time. This means that the peaks and troughs of their oscillations occur at the same time, which can happen in a wide range of physical systems (Pikovsky et al., 2001; Strogatz, 2003). The generalized phase difference (GPD) method was derived to identify phase synchronization based on the physical properties of coupled oscillatory systems (Rosenblum et al., 2001). In practice, according to Pikovsky et al. (2001), the presence of a horizontal plateau in the phase difference versus time diagram is the simplest way to evidence synchronization. In general, for two time series $x(t)$ and $y(t)$, their instantaneous phases $\phi_x(t)$ and $\phi_y(t)$, can be estimated using the analytic signal method expressed as (Gabor, 1910; Panter, 1965),

$$Z_x(t)=x(t)+i\tilde{x}(t)=A_x^H(t)e^{i\phi_x^H(t)}, \tag{1}$$

where $\tilde{x}$ is the Hilbert transform (HT) of $x(t)$ defined as,

$$\tilde{x}(t)=\frac{1}{\pi}\text{p.v.}\int_{-\infty}^{\infty}\frac{x(t')}{t-t'}dt', \tag{2}$$

where p.v denotes Cauchy's principal value.

From $Z_x(t)$ it is possible to calculate the instantaneous phase $\phi_x(t)$ as,

$$\phi_x^H(t)=\arctan\frac{Im(Z_x)}{Re(Z_x)}, \tag{3}$$

The instantaneous phase of $y(t)$, $\phi_y(t)$, can be calculated using a similar procedure. It is worth noting that HT is a non-parametric method and that the estimation of $\phi_x(t)$ and $\phi_y(t)$ based on the analytic signal (Equation 1) is comparable with a technique based on wavelets (Quyen et al., 1999).

Finally, denoting $\phi_x^H(t)=\phi_x$ and $\phi_y^H(t)=\phi_y$, the GPD can be expressed as,

$$\phi_{n,m}=n\phi_x-m\phi_y, \tag{4}$$

which in turn allows defining that $n:m$ *phase locking* appears if,

$$|\phi_{n,m}-s|<c, \tag{5}$$

where $c<2\pi$ and s is the average phase between the two time series $x(t)$ and $y(t)$ (Rosenblum et al., 2001). However, for noisy oscillators, non-stationary processes, or time series with oscillations at several frequency bands, the phase difference $\phi_{n,m}$ can be unbounded due to phase jumps. This means that synchronization is not necessarily evidenced as a continuous plateau in the phase difference versus time diagram and the condition (Equation 5) is not valid anymore. Notwithstanding, if the probability mass distribution of the *cyclic relative phase*

$$\Phi_{n,m}=\phi_{n,m}mod(2\pi), \tag{6}$$

has a dominating peak around a preferential value it indicates phase synchronization in a statistical sense (Rosenblum et al., 2001). A stable phase locking in a ratio $n:m$ means n cycles of the oscillator x and m cycles of the oscillator y. Furthermore, $\Phi_{1,1}$ near to 0 or 2π means that signals are in phase, values around $\pi/2$ means that signals are in quadrature, and $\Phi_{1,1}$ near to π means that signals are anti-phased.

On the one hand, the GPD method has the following advantages: (i) phase analysis allows, by means of $\phi_{n,m}$ plots, tracing transitions between qualitatively different regimes that are due to non-stationarity in the parameters of interacting systems and/or coupling, and (ii) it is possible to apply this method even to very short records. On the other hand, the method has disadvantages such as (i) the synchronous regimes of order different from $n:m$ show no synchrony, (ii) there are no straightforward methods to determine the integers n and m; thus, they need to be identified by trial and error or expert knowledge and (iii) if the noise is relatively strong, this method becomes ineffective and may even be misleading (Pikovsky et al., 2001).

We aim to investigate the PS characteristics between ENSO (System 1) and the inter-annual variability of precipitation over the NSA and FEP (System 2). Our goal is to characterize and quantify the seasonal and spatial PS patterns between both systems during EN and LN. Hypothetically, we consider that ENSO is the driving system and that precipitation is the response system (the influenced system).

4.3.1 | Strength of phase synchronization

Among several *n:m synchronization indices* that have been proposed in the literature (e.g., Rosenblum et al., 2001), we use the strength of PS defined as,

$$\chi_{n,m}=\left|\left\langle e^{i\left(n\phi_x-m\phi_y\right)}\right\rangle\right|, \tag{7}$$

The notation $\langle\cdot\rangle$ denotes temporal averaging. The index χ_t varies from 0 to 1, $\chi=0$ indicates that the phases of the two time series are completely independent, whereas $\chi=1$ indicates perfect phase synchronization (Rosenblum et al., 2001; Stein et al., 2014). Then, to analyse the evolution of χ throughout the year, we calculate χ for each season.

Our study requires the implementation of a statistical test to assess the significance of the PS values between systems X and Y. In our case, X represents the ENSO system and Y denotes the climatic variables in the study region. We consider the original system X and a representative number of possible states of the system Y, which represent independent copies of the underlying system, the so-called synthetic time series (STS), or surrogates. To construct the STS from system Y, we use permutations of the data points of the original time series Y while carefully preserving the seasonality of the time series. That is, we permute the data points in separate subsets for each month. For example, we took all data points for January and shuffled them randomly; after repeating this for all months, we reconstructed a synthetic time series.

The null hypothesis is that each STS is an independent realization of system Y, corresponding to a different initial condition or possible time series of the same system. To test the statistical significance of the strength of PS, χ, among X and Y, we generate 500 STSs of the Y system and obtain a test distribution of χ calculated with the observations of the system X and each STS of Y. Finally, we constructed the upper 95% confidence interval based on the 95th percentile of the test distribution. Then, when values fall outside the confidence band represent the ones where the null hypothesis is rejected, or that the system X is in PS with system Y.

5 | RESULTS AND DISCUSSION

5.1 | Climatic anomalies in the region of study

Figure 2 illustrates the sea surface temperature anomalies (SSTA) and surface pressure anomalies (SPAs) over NSA and FEP. During EN (LN) events, the central Pacific Ocean (the Niño 3.4 region) shows positive (negative) SSTAs while SPAs are negative (positive) (Bjerknes, 1969; Gill, 1980; Lindzen & Nigam, 1987; Wang & Picaut, 2004). Figure 2 (left column) shows a consistent weakening of the Walker circulation pattern during EN, characterized by warmer waters in the centre Pacific and deep convection in this region (negative SPAs), coinciding with a downward (or weakened) wind branch of the Walker cell over NSA that suppresses convection (positive SPAs) (Lau & Yang, 2015; Wang et al., 2017). In contrast, Figure 2 (right column) shows consistent strengthening of the Bjerkness feedback, exhibiting warmer waters, convection in the west (negative SPAs), and increased sea surface pressures in the central Pacific. This feature leads to a deeper thermocline in the west and a shallower thermocline in the east (Lau & Yang, 2015; Wang et al., 2017). Particularly over inland NSA, during EN (LN), the Caribbean exhibits positive (negative) anomalies of SST in DJF and MAM with predominant negative SPAs. In addition, during EN (LN), the Tropical North Atlantic (TNA) exhibits high positive (negative) SSTAs in MAM with predominant negative SPAs. These seasonal features cannot be explained entirely in terms of the Walker circulation as we discuss below.

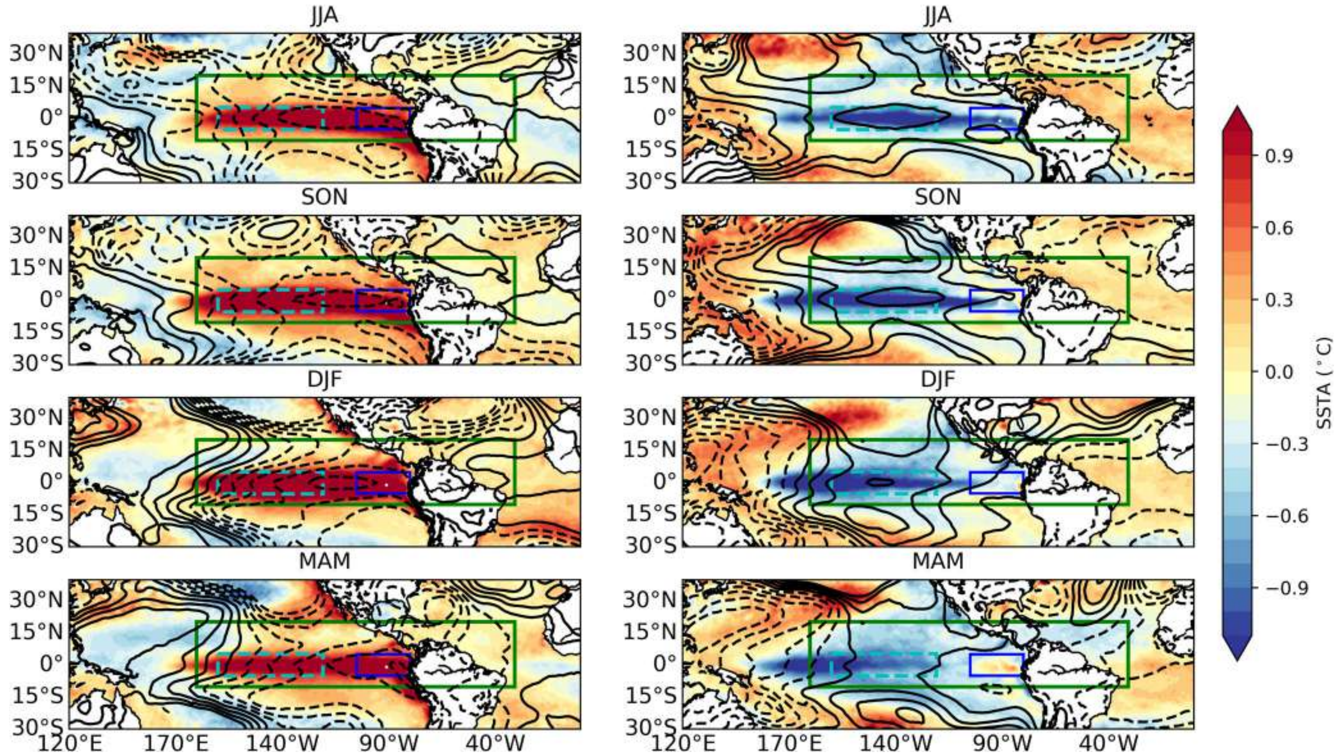

FIGURE 2 Composite of sea surface temperature anomalies (SSTA) and surface pressure anomalies (SPAs) over the NSA and FEP. (left column) EN. (right column) LN. Positive (negative) SPAs are marked by a solid (dashed) black line. The green box marks the region of study (180° W–30° W;10° S–20° N), the cyan box the Niño 3.4 region (170° W–120° W;5° S–5° N) and the blue box the Far-eastern Pacific (FEP) zone (105° W–80° W and 5° S–5° N). [Colour figure can be viewed at wileyonlinelibrary.com]

Figure 3 shows the standardized rainfall anomalies in the study region. During EN (LN), the FEP exhibits positive (negative) rainfall anomalies for all seasons (being higher in MAM and JJA). These negative (positive) anomalies in precipitation are associated with the weakening (strengthening) of Walker circulation in the Central Pacific, which in turn enhances (suppresses) convection and produces negative (positive) SPAs, as we explained previously. Over the continental NSA, Central America, and the Caribbean, precipitation exhibits negative (positive) anomalies for all seasons (being higher in MAM and JJA). The understanding of these negative (positive) anomalies in precipitation over NSA remains incomplete, and previous works have linked them to a variety of mechanisms and processes at different spatial and temporal scales. These include the influence of ENSO on the low-level jets (Caribbean, Orinoco, Choco), the impact of Walker circulation, and the connections between large-scale circulation and regional hydroclimatic processes, among others (Arias et al., 2021; Builes-Jaramillo et al., 2023; Cerón et al., 2021; Marengo & Hastenrath, 1993; Poveda et al., 2011, 2020; Salas et al., 2020; Yoon & Zeng, 2010).

These contrasting rainfall anomalies during the ENSO states in the FEP and NSA zones had been reported previously in several works (Glantz & Ramirez, 2020; Mason & Goddard, 2001; Ropelewski & Halpert, 1987). We point out two further interesting results: (i) the Pacific Ocean shows significant rainfall anomalies during both states of ENSO for a latitudinal band located around the 120° W–130° W while the FEP does not show significant rainfall anomalies, and (ii) NSA exhibits significant rainfall anomalies over the two predominant zones that we denote as CAR and GUI. This result contrasts with those presented by Ropelewski and Halpert (1987); Mason and Goddard (2001); Glantz and Ramirez (2020) because they have shown the rainfall anomalies over NSA as a continuous area. Here, we find significant rainfall anomalies in CAR and GUI, whereas rainfall anomalies over the corridor of the Orinoco low-level Jet (Builes-Jaramillo et al., 2022a, 2022b) are not significant. Similar results were found for rainfall anomalies using the CMAP data (see Supplementary Material; Figure 3).

5.2 | Strength of phase synchronization between SSTs in the tropical Pacific Ocean and precipitation

5.2.1 | Analysis for the canonical ENSO states

Figure 4 presents phase relationships between the ONI index and inter-annual precipitation in the tropical Pacific Ocean (the Niño 3.4 region). The time series of

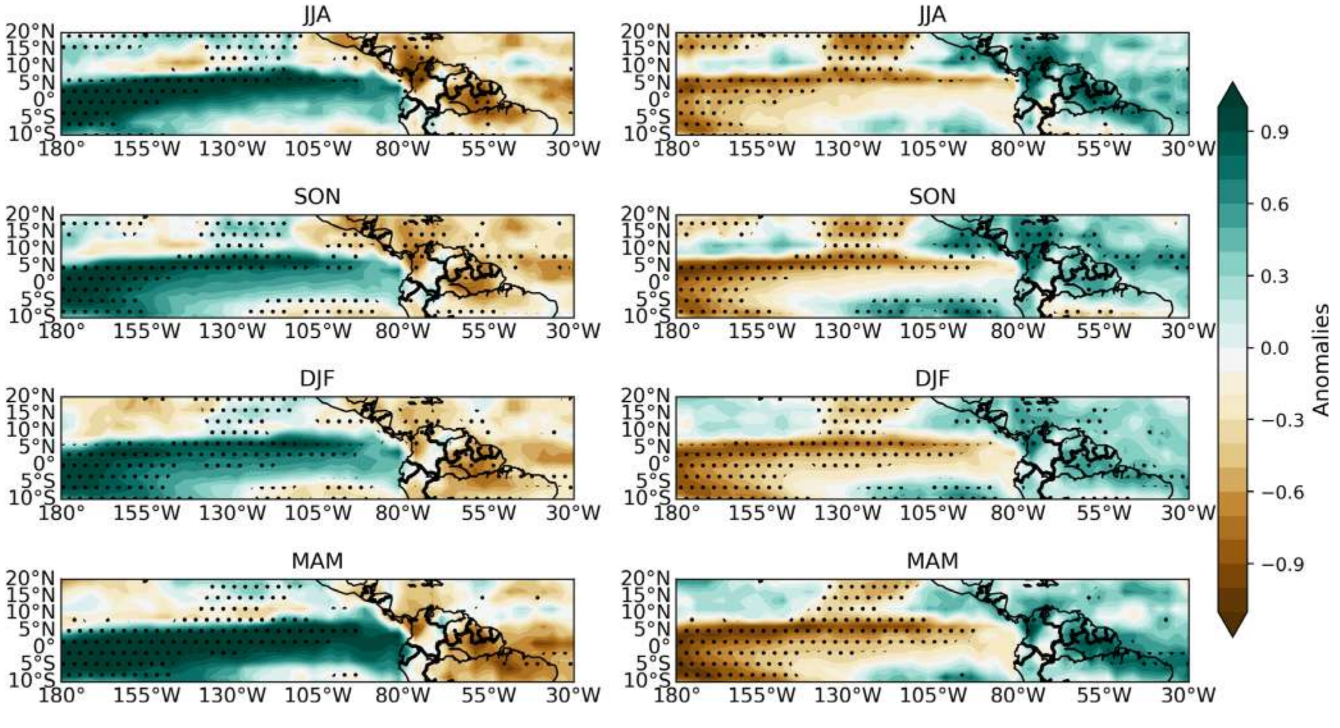

FIGURE 3 Standardized precipitation anomalies over the far eastern Pacific and northern South America according to GPCP. (left) Anomalies during EN. (right) Anomalies during LN. (Dots) zones where the change in precipitation anomalies is significant at the 0.05 level. [Colour figure can be viewed at wileyonlinelibrary.com]

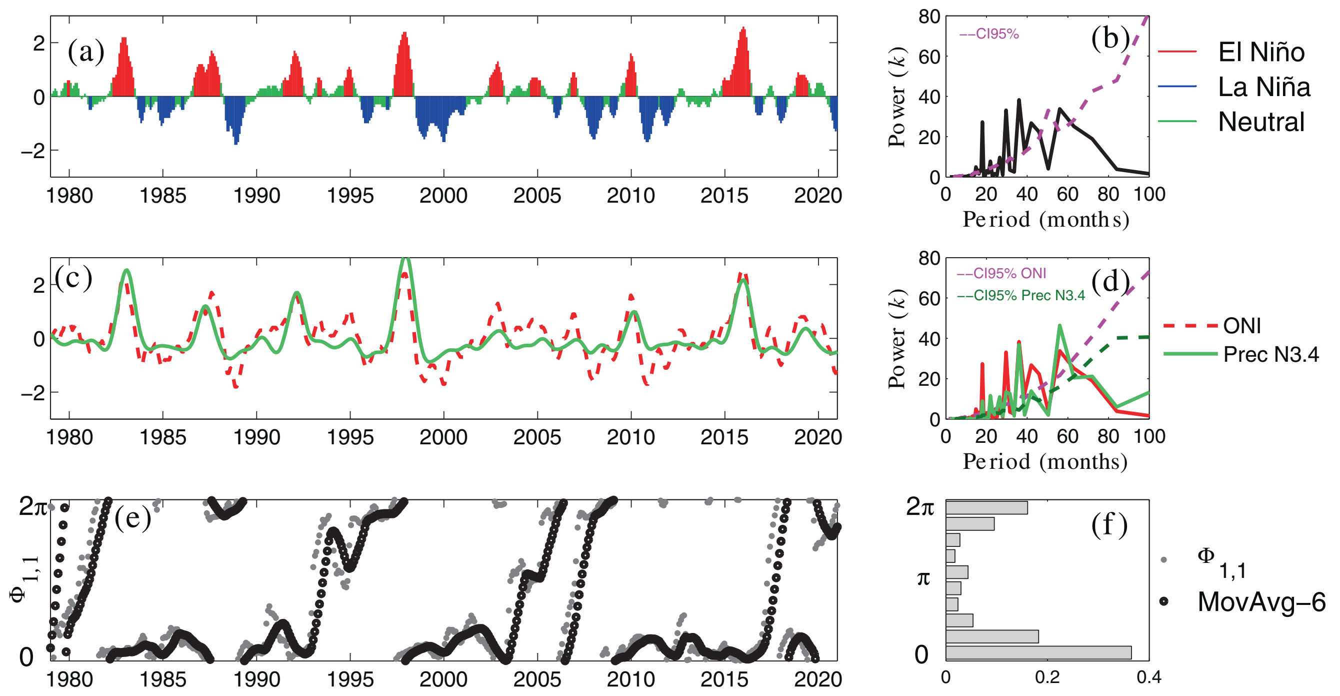

FIGURE 4 Phase relationship $\Phi_{1,1}$ between the ONI index and GPCP precipitation at the inter-annual frequency band in the Niño 3.4 region. (a) ONI index. (b) Periodogram of the ONI index. (c) Standardized time-series. (d) Periodograms of the time series. (e) Cylindrical representation of $\Phi_{1,1}$. (f) Relative frequency distribution computed using $\Phi_{1,1}$. Moving averages of $\Phi_{1,1}$ for illustrative purposes. In the periodograms, CI95% denotes the 95% confidence intervals assuming a red noise model. [Colour figure can be viewed at wileyonlinelibrary.com]

precipitation is obtained by spatially averaging the monthly precipitation fields (GPCP). Figure 4a shows the time series of the ONI index with red and blue denoting the occurrence of EN and LN events during the period 1979–2020, while Figure 4b provides its periodogram. Figure 4c shows the standardized time series (for the ONI index and precipitation at inter-annual timescales), and Figure 4d the periodograms for both ONI and precipitation in order to visualize the spectral composition of both signals, these periodograms show the 95% confidence intervals, which indicate that signals do not contain significant annual and intra-annual variability. Finally, Figure 4e shows the phase difference versus time diagram, $\Phi_{1,1}(t)$, while Figure 4f presents the probability mass distribution of the cyclic relative phases, which has preferential values around $\Phi_{1,1}(t) \approx 0$ or 2π. This result evidences that the SSTs and inter-annual precipitation are synchronized almost 80% of the time over the Niño 3.4 region, but with some periods of desynchronization such as March 1994–March 1995, July 2004–July 2008 and August 2018–December 2020. An analogous analysis was carried out for the CAR and GUI zones (see Supplementary Material; Figures 1 and 2). The CAR zone exhibits a preferential peak of $\Phi_{1,1}$ around π, which occurs approximately 60% of the time while GUI shows a less prominent peak of $\Phi_{1,1}$ around π, which occurs 40% of time. We point out that both CAR and GUI regions exhibit these preferential peak in $\Phi_{1,1}$ in the periods September 1986–July 1994, September 1994–July 2002 and July 2007–July 2016.

Figure 5 shows the strength of PS for the region of study for seasons DJF, MAM, JJA and SON. In general, we found that during both states of ENSO, the ONI index exhibits high PS with precipitation at inter-annual timescales in the Niño 3.4 region as well as the CAR and GUI zones. In terms of seasonality, during EN, PS is higher over the central Pacific in MAM and JJA, while over the CAR and GUI, it does not give a clear seasonal behaviour although PS is significant for all seasons. In contrast, during La Niña, PS is higher over the central Pacific zone with significant values for all seasons, while PS is higher in the CAR and GUI zones mainly in JJA. Moreover, the FEP zone does not show significant PS, which agrees with the weak linear relationship between the SST Niño 3.4 index and rainfall found by Jauregui and Takahashi (2018).

An interesting result is that while many regions with significant PS also experience significant precipitation anomalies, there are regions where significant PS occurs without corresponding precipitation anomalies, and vice versa. This suggests that ENSO may influence inter-annual precipitation variability in certain regions

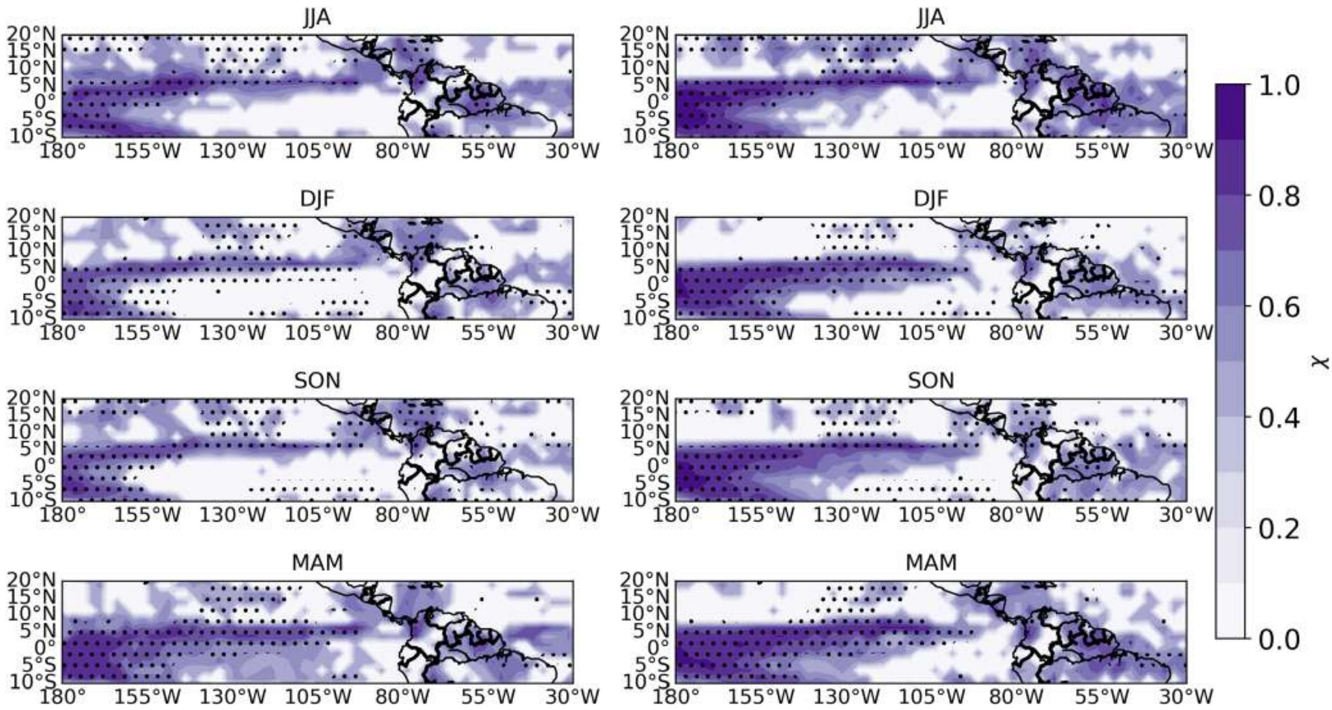

FIGURE 5 Strength of phase synchronization ($\chi_{1,1}$) between ONI and GPCP precipitation over the far-eastern Pacific and northern South America. (left column) EN. (right column) LN. (dots) Zones where precipitation anomalies are significant at the significance level of 0.05. (purple) Zones where χ is significant at 0.05. [Colour figure can be viewed at wileyonlinelibrary.com]

primarily in terms of phases rather than amplitudes (e.g., the CAR region in MAM during EN). This result opens new questions about the relationship between ENSO and precipitation, which may not be fully captured through composite analysis. Similar results were found for rainfall anomalies using the CMAP data (see Supplementary Material; Figure 3). Moreover, we obtain analogous results of PS between precipitation at inter-annual timescales and anomalies of SST in the Niño 3.4 region filtered using EEMD (see Supplementary Material; Figures 6 and 7). In general, we found spatial patterns similar to those found seasonally for the PS using a long-term approach for the periods of preferential peak in the probability mass of $\Phi_{1,1}$ (preferential values in the phase difference versus time diagram). However, precipitation anomalies do not show significant differences because both LN and EN events occur during such synchrony periods (not shown). Hence, the seasonal synchronization approach take relevance to investigate PS patterns as well as precipitation anomalies.

Our findings on phase synchronization patterns and precipitation anomalies during EN correspond to certain regions highlighted by Yun et al. (2021), particularly in the central Pacific, where positive precipitation anomalies occur during winter and spring. However, their focus is primarily on precipitation anomalies associated with shifts in the Walker and Hadley cells. Yun et al. (2021) propose that the shifts in the Walker and Hadley cells are not adequately captured by common ENSO indices such as the Niño 3 region. This disparity suggests that our research addresses distinct inquiries, leading to different results. Additionally, investigating the effects of Walker-Hadley synchronization on the precipitation of NSA and FEP falls outside the scope of our study.

5.2.2 | Analysis for different phases and types of ENSO

In general, there is a higher phase synchronization between the EP EN index and precipitation over the study region for all seasons (Figure 6). According to Timmermann et al. (2018), a large eastward shift of Pacific convection occurs during EP EN, which could be associated with the higher synchronization patterns found over FEP. This result agrees with previous evidence that precipitation anomalies for EP EN are higher than those experienced for CP EN for all seasons (Cai et al., 2020; Sullivan et al., 2016). The warmer (cooler) FEP waters during EP (CP) EN are related to a southward (northward) migration of the eastern Pacific ITCZ (Capotondi et al., 2015; Huaman & Schumacher, 2018; Zheng et al., 2014), which could be related to a greater PS near FEP and south (north) of the equator. Rainfall anomalies

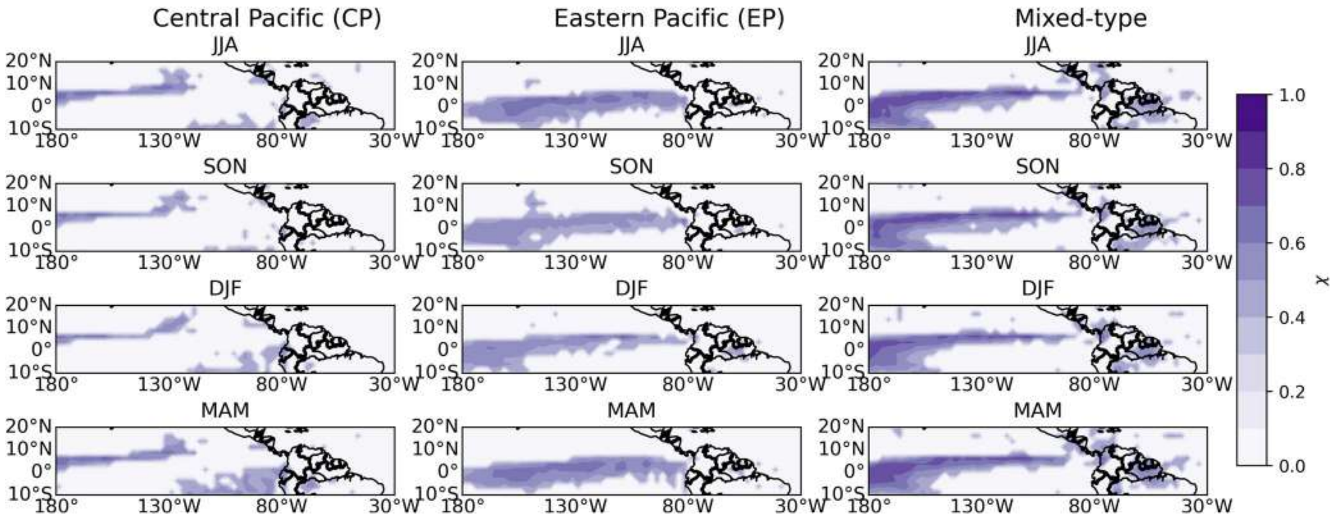

FIGURE 6 Strength of phase synchronization ($\chi_{1,1}$) between GPCP precipitation and the Indices for different types of EN. (left column) CP EN, (centre column) EP EN, (left column) Mixed-type EN. (purple) Zones where χ is significant at 0.05. [Colour figure can be viewed at wileyonlinelibrary.com]

during CP and EP EN types in NSA are due to the anomalous displacement of the Walker Cell (Cai et al., 2020; Hu et al., 2016; Sulca et al., 2024; Tedeschi & Collins, 2016). For CP EN, there is dryness (negative precipitation anomalies) over NSA due to anomalous sinking motion and divergent moisture transport. During EP EN, this motion moves towards the northern Amazon Basin, allowing for positive anomalies over FEP and the coasts of Peru and Ecuador (Andreoli et al., 2017). According to Gushchina et al. (2020), there is a weak response to the CP EN signal in terms of dryness indices over the tropical surface when compared with the response during the EP EN. Those studies are consistent with our findings for precipitation (see Figure 4; Supplementary Material). Furthermore, the previous literature suggest that for EP EN, a higher impact on precipitation can be expected over the coasts of Colombia, Ecuador and Peru, resulting in higher anomalies than those experienced during CP EN. Notwithstanding, the tropical Andes regions exhibit particularities that deserve further research in terms phase synchronization, which are out of the scope of this work. In this sense, Segura et al. (2019) shows that precipitation in the southern tropical Andes (20° S–8° S) is primarily influenced by sea surface temperature (SST) variability over the central Pacific. However, in the transition Andes (8° S–5° S), this SST variability (e.g., February–April during EN and LN) is not the primary factor. Dry events in the transition Andes are associated with an intensification of the eastern branch of the Walker cell, while wet events are linked to increased convection over the equatorial Amazon (Segura et al., 2019).

Moreover, Figure 6 evidences that the magnitude of the strength of PS increases progressively from CP EN ($\chi \approx 0.4$), EP EN ($\chi \approx 0.6$) and the Mixed-type EN ($\chi \approx 0.8$), respectively. In addition, the areas of PS are less extensive for CP EN and larger for the Mixed-type EN. In this sense, the PS method enables us to unveil these patterns over the study region, which coincide with those reported in the literature (Andreoli et al., 2017; Gushchina et al., 2020; Takahashi & Martínez, 2019). Furthermore, for these CP and EP EN some regions of significant precipitation anomalies do not show significant PS.

5.3 | Strength of phase synchronization between SSTs in the tropical Pacific Ocean and low-level winds

Figure 7 shows the seasonal strength of PS between ONI and zonal wind speeds at 925 hPa. We found that during EN and LN, the ONI index is phase-locked with zonal wind speeds in most of the zones where precipitation also exhibits PS (Figure 5). In this sense, PS is stronger over the Niño 3.4 region, in the zones where a higher coincidence with precipitation can be expected for EP EN (see Figure 6). Additionally, those PS patterns resemble those discovered for zonal wind velocities at 850 hPa (not shown).

We found that during EN and LN in JJA and DJF, the winds are phase-locked with ONI over the area of the CLLJ, over the Caribbean Sea, the Andean region of Colombia, Central America and the tropical Pacific

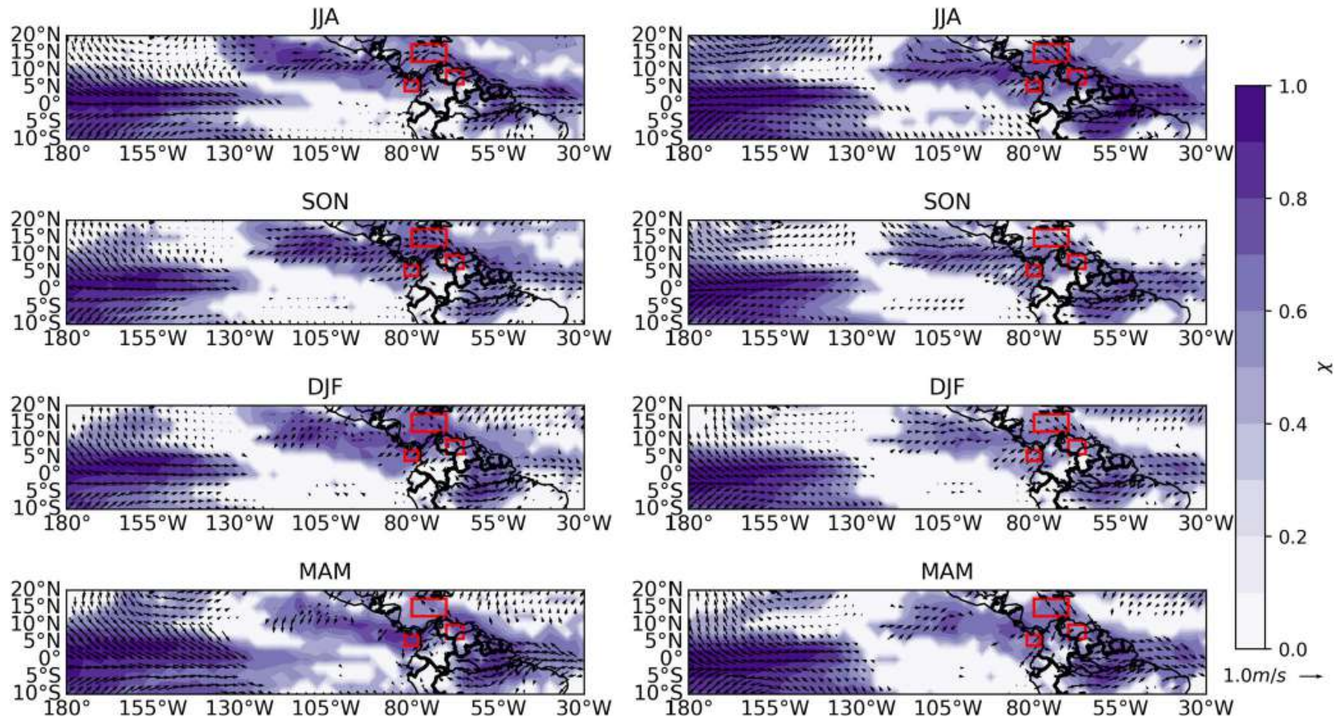

FIGURE 7 Strength of phase synchronization ($\chi_{1,1}$) between ONI and zonal wind speed anomalies at 925 hPa from ERA5 atmospheric reanalysis. (left column) EN. (right column) LN. (vectors) zones where anomalies of zonal winds are significant at the significance level of 0.05. (red boxes) areas associated with Low-level jets. (purple) Zones where χ is significant at 0.05. [Colour figure can be viewed at wileyonlinelibrary.com]

Ocean around latitude 5° N. During these seasons, the increase (decrease) of the CLLJ winds is related to the increase (decrease) of wind divergences over these regions resulting in less (more) precipitation than normal (Wang, 2007) (see Figure 3). In addition, wind speeds at 925 hPa are phase-locked with ONI also for seasons when the CLLJ is not in its maximum activity. In contrast, CLLJ winds and precipitation are phase-locked mainly during EN over the Caribbean and the Andes mountains of Colombia whereas during LN such PS only is evidenced in JJA (see Figure 5; Supplementary Material).

For the OLLJ in DJF (its season of activity), we found that during EN and LN, there is PS between ONI and OLLJ winds at the entrance of the OLLJ. However, over the corridor of the OLLJ, there is no evidence of PS for both ENSO states. Furthermore, we found that during EN and LN, the OLLJ winds are not PS with precipitation in the Orinoco plains of Colombia. These results can be explained because during EN (LN) the OLLJ winds decrease (increase) their frequency of occurrence, and there is a decrease (increase) in the water vapour flux over the corridor of the OLLJ. Particularly, in the OLLJ corridor, precipitation slightly decreases for both ENSO states without a clear pattern of alteration (Builes-Jaramillo et al., 2022a, 2022b).

For the ChocoJet in SON (its season of activity), we found that during EN (LN), the ChocoJet winds are in PS with ONI. We also found coherence with our analysis of PS between ChocoJet winds and precipitation (see Figure 5; Supplementary Material). These results can be explained because during EN (LN) the ChocoJet winds decrease (increase) and this behaviour has been associated with a decrease (increase) of precipitation over the western Colombian Pacific (Poveda et al., 2011; Poveda & Mesa, 2000; Yepes et al., 2019).

5.4 | Phase differences

Figure 8 shows the seasonal phase difference $\phi_{1,1}$ between the phases of the ONI index and precipitation during EN and LN. This phase difference only makes sense in zones where the strength of PS is significant (hatched areas in the Figure 8) according to Section 4.3 because PS occurs only when the phase difference exhibits a dominating peak around a preferential value. During EN for all seasons, Figure 8 (left column) shows that STAs and precipitation are in-phase ($\phi_{1,1}$ near to 0 or 2π) over the Niño 3.4 region. Furthermore, CAR exhibits a phase difference ($\phi_{1,1}$ ranging from $\pi/2$ to π) that suggest a transition between quadrature and anti-

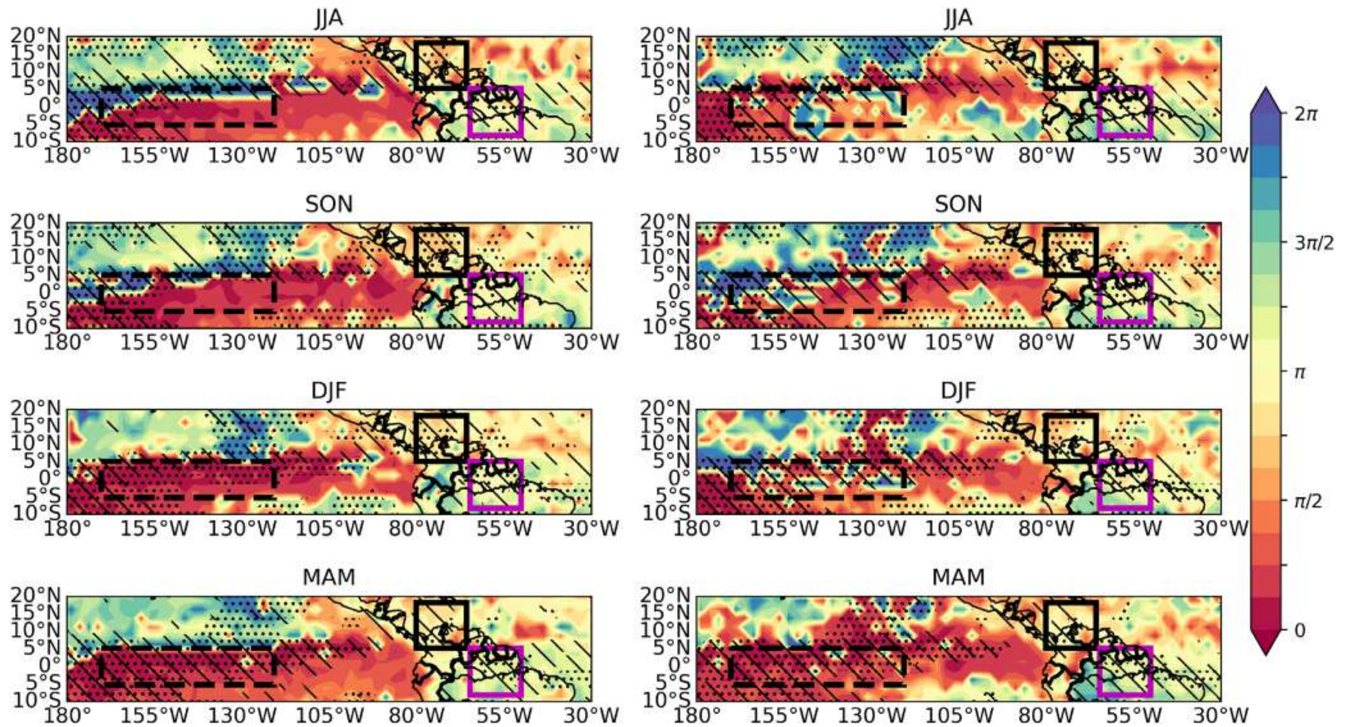

FIGURE 8 Phase difference between the phases of the ONI index and precipitation during ENSO over the far-eastern Pacific and northern South America. (left column) EN. (right column) LN. (dots) Zones where anomalies of precipitation are significant. (hatched) Zones where the strength of PS is significant. [Colour figure can be viewed at wileyonlinelibrary.com]

phased behaviour. Moreover, GUI shows that signals are anti-phased ($\phi_{1,1}$ near to π). During LN, Figure 8 (right column) exhibits phase difference patterns analogous to those observed during EN. Notwithstanding, the phase difference patterns for LN show higher variability than for EN. Similar results were found for phase differences using the CMAP data (not shown).

6 | FINAL REMARKS AND FUTURE WORK

By means of phase synchronization techniques and composite analysis, we have found that seasonal anomalies of climatic variables in the FEP and NSA during EN and LN states are consistent with those provided by the body of the literature. Notwithstanding, we found important particularities over the NSA patterns of surface temperatures and surface pressure. In particular, the Caribbean (CAR zone) and the Guianas (GUI zone) exhibit interesting features. During EN, STAs are positive for all seasons and coincide with negative SPAs. During LN, STAs are positive in JJA and SON but negative in DJF and MAM; for this state of ENSO, SPAs are predominantly negative. In terms of seasonal precipitation anomalies, we found that all seasons exhibit significant changes during both states of ENSO. In particular, the central tropical Pacific (the Niño 3.4 region), CAR and GUI zones exhibit higher significant anomalies of precipitation. During EN (LN), the Niño 3.4 region experiences positive (negative) anomalies, while the CAR and GUI zones exhibit negative (positive) ones. These results had been reported by Ropelewski and Halpert (1987), Mason and Goddard (2001), Glantz and Ramirez (2020), although none of these works emphasized that NSA does not show significant changes in precipitation anomalies in the corridor of the Orinoco low-level jet. These results coincide with results reported by Jones (2019) but contrast with finding presented in other works (Builes-Jaramillo et al., 2022a, 2022b; Salas, 2020). Furthermore, the tropical Pacific Ocean presents a band of significant precipitation anomalies during the states of ENSO around the longitude 105° W–130° W and latitudes 5° N–20° N. These features deserve future research. When analysing the PS between precipitation and the CP and EP EN indices, the strength of phase-locking is more evident for the EP EN in all seasons, showing also the synchronization in the areas where the ITCZ is reported to migrate during this non-canonical ENSO events. These particular results show the capability of the PS technique to unveil the response of precipitation to CP and EP as found previously (Andreoli et al., 2017; Capotondi et al., 2015; Sullivan et al., 2016; Tedeschi & Collins, 2016). Moreover, our results showed that the magnitude of the strength of PS increases progressively from CP EN, EP EN and the mixed-type EN, respectively.

Most regions with significant PS correspond to areas exhibiting significant changes in precipitation anomalies. However, in the Orinoco and northern Amazon River basins, significant PS occurs without significant changes in precipitation anomalies. This result allows us to hypothesize that while the ENSO signal may be associated with precipitation phases in some regions, it might not affect precipitation in terms of amplitude. This insight prompts new research avenues into the influence of ENSO states on precipitation, as classical composite analysis mainly focuses on anomaly patterns in terms of magnitudes, leaving the timing of climate variables relatively understudied. Furthermore, we study PS between LLJ winds at 925 hPa and precipitation. In particular, we use zonal winds in regions associated with the CLLJ, the OLLJ, and the ChocoJet. Our results confirm that during EN, the phases of the CLLJ winds (JJA and DJF) are related to a decrease in precipitation in the region, whereas during LN, there is no evidence of PS (Wang, 2007). The OLLJ winds do not exhibit PS with precipitation in the Orinoco region for either state of ENSO. The ChocoJet winds show PS with precipitation over western Colombia for both states of ENSO, which can be associated with the increase (decrease) in ChocoJet winds during LN (EN) and the increase (decrease) in precipitation over western Colombia (Poveda & Mesa, 2000). Finally, some PS spatial patterns for precipitation and low-level winds at 925 hPa are coincident over the LLJ regions, these results suggest phase synchrony between low-level winds and precipitation, relationship that have been mentioned using other approaches for each LLJ case by Wang (2007); Poveda and Mesa (2000); Builes-Jaramillo et al. (2022a, 2022b).

Our analysis of PS aligns with findings widely reported in the literature regarding inter-annual time scales. However, PS offers a distinct perspective on the influence of ENSO on rainfall variability in the FEP and NSA regions. Given its non-linear nature, the PS method facilitates quantifying relationships between oscillatory processes across diverse time scales, such as the interannual variability of ENSO and the annual precipitation cycle, and the inter-annual variability of ENSO and the Pacific decadal oscillation (PDO). In this sense, this work opens new questions for future work: (i) Stein et al. (2014) proposed an ENSO seasonal synchronization theory but, what are the patterns of PS between the inter-annual variability of ENSO in the tropical Pacific Ocean and the annual variability of precipitation over the FEP and NSA?; (ii) Is there a significant PS between the PDO and ENSO in the FEP and NSA? Do they offer new information about the climate anomalies in FEP and NSA? (Rojas-Murillo et al., 2021); (iii) Our results evidenced that over the Pacific Ocean, North Atlantic Ocean, and Southeastern Brazil, there is PS but not necessarily a change in the magnitude of the precipitation anomalies, remaining the questions: Which are the timing features or non-direct pathways through other processes of the hydroclimatic variables in this region during ENSO?; Does desynchronization occur during ENSO transitions from Neutral to EN or Neutral to LN? How are PS patterns during the ENSO transitions? Further research is needed about the phase synchronization features during the ENSO transitions (Builes-Jaramillo et al., 2023); (iv) What is the influence of the Walker-Hadley synchronization on precipitation of NSA and FEP?; (v) How could change synchronization patterns on ENSO under climate change? Recent literature suggests that ENSO teleconnections could vary substantially under the influence of global warming (Alizadeh, 2024) and (vi) How are the patterns of synchronization between the Amazon convection and precipitation in the tropical Andes? Segura et al. (2019) found relationships between those processes but a synchronization approach is an open topic.

AUTHOR CONTRIBUTIONS

Hernán D. Salas: Conceptualization; methodology; software; data curation; formal analysis; investigation; writing – original draft; visualization; writing – review and editing. **Alejandro Builes-Jaramillo:** Conceptualization; methodology; software; formal analysis; investigation; writing – original draft; writing – review and editing. **Niklas Boers:** Conceptualization; supervision; writing – original draft; writing – review and editing. **Germán Poveda:** Conceptualization; supervision; writing – review and editing. **Óscar J. Mesa:** Conceptualization; supervision; writing – review and editing. **Jürgen Kurths:** Conceptualization; writing – review and editing; supervision; funding acquisition; methodology.

ACKNOWLEDGEMENTS

The work of H. D. Salas was partially funded by COLCIENCIAS (Grant for National Doctorates 617-2), Humboldt University of Berlin IRTG 1740, Institución Universitaria Colegio Mayor de Antioquia (projects FAI54 and FAI65) and Instituto Tecnológico Metropolitano. The work of A. Builes-Jaramillo is supported by Institución Universitaria Colegio Mayor de Antioquia. N. Boers acknowledges funding from the Volkswagen Foundation. The work of G. Poveda and O. J. Mesa is supported by Universidad Nacional de Colombia at Medellin. The work by J. Kurths is supported by PIK. Thanks to the European Centre for Medium-Range Weather Forecast ECMWF for the ERA5 datasets and NOAA for the ENSO index data. Thanks to the anonymous reviewers for their suggestions and recommendations to improve this work.

FUNDING INFORMATION

The work was funded by COLCIENCIAS (Grant for National Doctorates 617-2), Humboldt University of Berlin IRTG 1740, Institución Universitaria Colegio Mayor de Antioquia (Projects FAI54 and FAI65), Universidad Nacional de Colombia—Sede Medellín, Volkswagen Foundation, and Departamento de Ciencias Ambientales y de la Construcción, Facultad de Ciencias Exactas y Aplicadas, Instituto Tecnológico Metropolitano, Medellín, Colombia.

CONFLICT OF INTEREST STATEMENT

The authors declare no conflicts of interest.

DATA AVAILABILITY STATEMENT

The data sets used in this study are available online. ERA5 atmospheric reanalysis (Dataset) Hersbach et al. (2019) is available at https://cds.climate.copernicus.eu/cdsapp#!/dataset/reanalysis-era5-single-levels-monthly-means. The Oceanic Niño Index (ONI) is available at https://origin.cpc.ncep.noaa.gov/products/analysis_monitoring/ensostuff/ONI_v5.php. The Global Precipitation Climatological Project (GPCP) data set is available on the website https://psl.noaa.gov/data/gridded/data.gpcp.html. The CPC Merged Analysis of Precipitation (CMAP) data set is available on the website https://psl.noaa.gov/data/gridded/data.cmap.html.

ORCID

Hernán D. Salas https://orcid.org/0000-0002-6182-237X
Alejandro Builes-Jaramillo https://orcid.org/0000-0002-3474-6922

REFERENCES

Adler, R., Sapiano, M., Huffman, G., Wang, J.-J., Gu, G., Bolvin, D. et al. (2018) The global precipitation climatology project (GPCP) monthly analysis (new version 2.3) and a review of 2017 global precipitation. *Atmosphere*, 9, 138. Available from: http://www.mdpi.com/2073-4433/9/4/138

Ahdesmäki, M., Lähdesmäki, H., Pearson, R., Huttunen, H. & Yli-Harja, O. (2005) Robust detection of periodic time series measured from biological systems. *BMC Bioinformatics*, 6, 117. Available from: https://doi.org/10.1186/1471-2105-6-117

Alizadeh, O. (2024) A review of enso teleconnections at present and under future global warming. *WIREs Climate Change*, 15, 1–20.

Andreoli, R.V., de Oliveira, S.S., Kayano, M.T., Viegas, J., de Souza, R.A.F. & Candido, L.A. (2017) The influence of different El Niño types on the south American rainfall. *International Journal of Climatology*, 37, 1374–1390.

Andreoli, R.V. & Kayano, M.T. (2005) Enso-related rainfall anomalies in south america and associated circulation features during warm and cold pacific decadal oscillation regimes. *International Journal of Climatology*, 25, 2017–2030.

Arias, P.A., Garreaud, R., Poveda, G., Espinoza, J.C., Molina-Carpio, J., Masiokas, M. et al. (2021) Hydroclimate of the andes part ii: hydroclimate variability and sub-continental patterns. *Frontiers in Earth Science*, 8, 1–25. Available from: https://doi.org/10.3389/feart.2020.505467/full

Bedoya-Soto, J.M., Poveda, G., Trenberth, K.E. & Vélez-Upegui, J.J. (2019) Interannual hydroclimatic variability and the 2009–2011 extreme enso phases in Colombia: from andean glaciers to caribbean lowlands. *Theoretical and Applied Climatology*, 135, 1531–1544.

Bjerknes, J. (1969) Atmospheric teleconnections from the equatorial Pacific. *Monthly Weather Review*, 97, 163–172. Available from: https://doi.org/10.1175/1520-0493(1969)097%3C0163:ATFTEP%3E2.3.CO;2

Boschat, G., Simmonds, I., Purich, A., Cowan, T. & Pezza, A.B. (2016) On the use of composite analyses to form physical hypotheses: an example from heat wave - SST associations. *Scientific Reports*, 6, 1–10. Available from: https://www.exelisvis.com/

Brown, R. & Kocarev, L. (2000) A unifying definition of synchronization for dynamical systems. *Chaos: An Interdisciplinary Journal of Nonlinear Science*, 10, 344–349.

Builes-Jaramillo, A., Valencia, J. & Salas, H.D. (2023) The influence of the El Niño-southern oscillation phase transitions over the northern South America hydroclimate. *Atmospheric Research*, 290, 106786. Available from: https://linkinghub.elsevier.com/retrieve/pii/S0169809523001837

Builes-Jaramillo, A., Yepes, J. & Salas, H.D. (2022a) The orinoco low-level jet and its association with the hydroclimatology of northern south america. *Journal of Hydrometeorology*, 23, 209–223.

Builes-Jaramillo, A., Yepes, J. & Salas, H.D. (2022b) The orinoco low-level jet during el niño–southern oscillation. *International Journal of Climatology*, 42, 7863–7877. Available from: https://doi.org/10.1002/joc.7681

Cai, W., McPhaden, M.J., Grimm, A.M., Rodrigues, R.R., Taschetto, A.S., Garreaud, R.D. et al. (2020) Climate impacts of the el niño-southern oscillation on south america. *Nature Reviews Earth and Environment*, 1, 215–231.

Capotondi, A., Wittenberg, A.T., Newman, M., Di Lorenzo, E., Yu, J.Y., Braconnot, P. et al. (2015) Understanding enso diversity. *Bulletin of the American Meteorological Society*, 96, 921–938.

Cerón, W.L., Kayano, M.T., Andreoli, R.V., Canchala, T., Carvajal-Escobar, Y. & Alfonso-Morales, W. (2021) Rainfall variability in southwestern Colombia: changes in enso-related features. *Pure and Applied Geophysics*, 178, 1087–1103.

Chen, N., Thual, S. & Stuecker, M.F. (2019) El niño and the southern oscillation: theory.

Díaz, D.C. & Villegas, N. (2022) Wavelet coherence between enso indices and two precipitation database for the andes region of Colombia. *Atmosfera*, 35(2), 237–271.

Freund, M.B., Henley, B.J., Karoly, D.J., McGregor, H.V., Abram, N.J. & Dommenget, D. (2019) Higher frequency of Central Pacific El Niño events in recent decades relative to past centuries. *Nature Geoscience*, 12, 450–455. Available from: https://doi.org/10.1038/s41561-019-0353-3

Friedman, A.R., Bollasina, M.A., Gastineau, G. & Khodri, M. (2021) Increased amazon basin wet-season precipitation and river discharge since the early 1990s driven by tropical pacific variability. *Environmental Research Letters*, 16, 1–11.

Gabor, D. (1910) Theory of communication. *Journal of the Institution of Electrical Engineers*, 93, 429–457.

Geng, T., Cai, W., Wu, L., Santoso, A., Wang, G., Jing, Z. et al. (2022) Emergence of changing Central-Pacific and eastern-Pacific El Niño-southern oscillation in a warming climate. *Nature Communications*, 13, 1–11.

Ghil, M., Allen, M.R., Dettinger, M.D., Ide, K., Kondrashov, D., Mann, M.E. et al. (2002) Advanced spectral methods for climatic time series. *Reviews of Geophysics*, 40, 3-1–3-41. Available from: https://doi.org/10.1029/2000RG000092

Gill, A.E. (1980) Some simple solutions for heat-induced tropical circulation. *Quarterly Journal of the Royal Meteorological Society*, 106, 447–462. Available from: https://doi.org/10.1002/qj.49710644905

Glantz, M.H. & Ramirez, I.J. (2020) Reviewing the oceanic niño index (oni) to enhance societal readiness for el niño's impacts. *International Journal of Disaster Risk Science*, 11, 394–403.

Grimm, A.M. & Tedeschi, R.G. (2009) Enso and extreme rainfall events in south america. *Journal of Climate*, 22, 1589–1609.

Gushchina, D., Zheleznova, I., Osipov, A. & Olchev, A. (2020) Effect of various types of ENSO events on moisture conditions in the humid and subhumid tropics. *Atmosphere*, 11, 1–24.

Hersbach, H., Bell, B., Berrisford, P., Horányi, A., Sabater, J.M., Nicolas, J. et al. (2019) Global reanalysis: goodbye ERA-interim, hello ERA5. *ECMWF Newsletter*, 159, 17–24.

Hu, X., Yang, S. & Cai, M. (2016) Contrasting the eastern Pacific El Niño and the central Pacific El Niño: process-based feedback attribution. *Climate Dynamics*, 47, 2413–2424.

Huaman, L. & Schumacher, C. (2018) Assessing the vertical latent heating structure of the east pacific ITCZ using the CloudSat CPR and TRMM PR. *Journal of Climate*, 31, 2563–2577.

Huang, N.E., Shen, Z., Long, S.R., Wu, M.C., Shih, H.H., Zheng, Q. et al. (1998) The empirical mode decomposition and the Hilbert spectrum for nonlinear and non-stationary time series analysis. *Proceedings of the Royal Society of London, Series A: Mathematical, Physical and Engineering Sciences*, 454, 903–995. Available from: https://doi.org/10.1098/rspa.1998.0193

Huang, N.E. & Wu, Z. (2008) A review on Hilbert-Huang transform: method and its applications to geophysical studies. *Reviews of Geophysics*, 46, RG2006. Available from: https://doi.org/10.1029/2007RG000228

Huffman, G.J., Adler, R.F., Arkin, P., Chang, A., Ferraro, R., Gruber, A. et al. (1997) The global precipitation climatology project (GPCP) combined precipitation dataset. *Bulletin of the American Meteorological Society*, 78, 5–20. Available from: https://doi.org/10.1175/1520-0477(1997)078%3C0005:TGPCPG%3E2.0.CO;2

Jajcay, N., Kravtsov, S., Sugihara, G., Tsonis, A.A. & Paluš, M. (2018) Synchronization and causality across time scales in el niño southern oscillation. *npj Climate and Atmospheric Science*, 1, 33.

Jauregui, Y.R. & Takahashi, K. (2018) Simple physical-empirical model of the precipitation distribution based on a tropical sea surface temperature threshold and the effects of climate change. *Climate Dynamics*, 50, 2217–2237.

Jiménez-Sánchez, G., Markowski, P.M., Young, G.S. & Stensrud, D.J. (2020) The orinoco low-level jet: an investigation of its mechanisms of formation using the wrf model. *Journal of Geophysical Research: Atmospheres*, 125, 1–23.

Jones, C. (2019) Recent changes in the South America low-level jet. *npj Climate and Atmospheric Science*, 2, 20. URL:. Available from: http://www.nature.com/articles/s41612-019-0077-5

Kousky, V.E. & Higgins, R.W. (2007) An alert classification system for monitoring and assessing the ENSO cycle. *Weather and Forecasting*, 22, 353–371. Available from: https://doi.org/10.1175/WAF987.1

Kousky, V.E., Kagano, M.T. & Cavalcanti, I.F.A. (1984) A review of the southern oscillation: oceanic-atmospheric circulation changes and related rainfall anomalies. *Tellus A: Dynamic Meteorology and Oceanography*, 36, 490.

Lange, H., Sippel, S. & Rosso, O.A. (2018) Nonlinear dynamics of river runoff elucidated by horizontal visibility graphs. *Chaos: An Interdisciplinary Journal of Nonlinear Science*, 28, 075520. URL:. Available from: https://doi.org/10.1063/1.5026491

Lau, K.-M. & Yang, S. (2015) Walker circulation. In: Pyle, J., & Zhang, F. (Eds.) *Encyclopedia of Atmospheric Sciences*. Academic Press, Elsevier, pp. 177–181. https://shop.elsevier.com/books/encyclopedia-of-atmospheric-sciences/north/978-0-12-382225-3

Lindzen, R.S. & Nigam, S. (1987) On the role of sea surface temperature gradients in forcing low-level winds and convergence in the tropics. *Journal of the Atmospheric Sciences*, 44, 2418–2436.

Liu, J., Song, M., Hu, Y. & Ren, X. (2012) Changes in the strength and width of the hadley circulation since 1871. *Climate of the Past*, 8, 1169–1175.

Maraun, D. & Kurths, J. (2005) Epochs of phase coherence between el niño/southern oscillation and indian monsoon. *Geophysical Research Letters*, 32, L15709.

Marengo, J.A. & Hastenrath, S. (1993) Case studies of extreme climatic events in the amazon basin. *Journal of Climate*, 6, 617–627.

Mason, S.J. & Goddard, L. (2001) Probabilistic precipitation anomalies associated with ENSO. *Bulletin of the American Meteorological Society*, 82, 619–638. Available from: https://doi.org/10.1175/1520-0477(2001)082%3C0619:PPAAWE%3E2.3.CO;2

Matyasovszky, I. (2013) Estimating spectra of unevenly spaced climatological time series. *Quarterly Journal of the Hungarian Meteorological Service*, 117, 187–200.

McPhaden, M., Busalacchi, A. & Anderson, D. (2010) A toga retrospective. *Oceanography*, 23, 86–103.

Mejía, J.F., Yepes, J., Henao, J.J., Poveda, G., Zuluaga, M.D., Raymond, D.J. et al. (2021) Towards a mechanistic understanding of precipitation over the far eastern tropical pacific and western Colombia, one of the rainiest spots on earth. *Journal of Geophysical Research: Atmospheres*, 126, 1–23.

Mokhov, I.I., Smirnov, D.A., Nakonechny, P.I., Kozlenko, S.S., Seleznev, E.P. & Kurths, J. (2011) Alternating mutual influence of el-niño/southern oscillation and indian monsoon. *Geophysical Research Letters*, 38, n/a–n/a.

Neelin, J.D. & Su, H. (2005) Moist teleconnection mechanisms for the tropical south american and atlantic sector*. *Journal of Climate*, 18, 3928–3950.

Panisset, J.S., Libonati, R., Gouveia, C.M.P., Machado-Silva, F., França, D.A., França, J.R.A. et al. (2018) Contrasting patterns

of the extreme drought episodes of 2005, 2010 and 2015 in the amazon basin. *International Journal of Climatology*, 38, 1096–1104.
Panter, P.F. (1965) *Modulation, noise, and spectral analysis*. New York: McGraw Hill, p. 759
Pearson, R., Lähdesmäki, H., Huttunen, H. & Yli-Harja, O. (2003) Detecting periodicity in nonideal datasets. In: Barbar, D. & kamath, C. (Eds.) *Proceedings of the third SIAM international conference on data mining, San Francisco, CA, USA*, 1–3 May 2003, pp. 274–278, SIAM. https://doi.org/10.1137/1.9781611972733.29
Philander, S.G.H. (1983) El niño southern oscillation phenomena. *Nature*, 302, 295–301.
Pikovsky, A., Rosenblum, M. & Kurths, J. (2001) *Synchronization: A universal concept in nonlinear sciences*. New York: Cambridge University Press.
Poveda, G., Álvarez, D.M. & Rueda, Ó.A. (2011) Hydro-climatic variability over the andes of Colombia associated with enso: a review of climatic processes and their impact on one of the earth's most important biodiversity hotspots. *Climate Dynamics*, 36, 2233–2249.
Poveda, G., Espinoza, J.C., Zuluaga, M.D., Solman, S.A., Garreaud, R. & van Oevelen, P.J. (2020) High impact weather events in the Andes. *Frontiers in Earth Science*, 8, 1–32. Available from: https://doi.org/10.3389/feart.2020.00162/full
Poveda, G. & Mesa, O.J. (2000) On the existence of lloró (the rainiest locality on earth): enhanced ocean-land-atmosphere interaction by a low-level jet. *Geophysical Research Letters*, 27, 1675–1678.
Quyen, M.L.V., Martinerie, J., Adam, C. & Varela, F.J. (1999) Nonlinear analyses of interictal EEG map the brain interdependences in human focal epilepsy. *Physica D: Nonlinear Phenomena*, 127, 250–266. Available from: https://linkinghub.elsevier.com/retrieve/pii/S0167278998002589
Rasmussen, E.M. & Wallace, J.M. (1983) Meteorological aspects of the El Niño/southern oscillation. *Science*, 222, 1195–1202. Available from: https://doi.org/10.1126/science.222.4629.1195
Rato, R., Ortigueira, M. & Batista, A. (2008) On the HHT, its problems, and some solutions. *Mechanical Systems and Signal Processing*, 22, 1374–1394. Available from: https://linkinghub.elsevier.com/retrieve/pii/S0888327007002701
Rojas-Murillo, K., Lupo, A.R., Garcia, M., Gilles, J., Korner, A. & Rivera, M.A. (2021) ENSO and PDO related interannual variability in the north and east-central part of the Bolivian altiplano in South America. *International Journal of Climatology*, 42(4), 2413–2439. Available from: https://doi.org/10.1002/joc.7374
Rojo, J.D. & Mesa, O.J. (2020) A simple conceptual model for the heat induced circulation over northern south america and meso-america. *Atmosphere*, 11, 1235.
Ropelewski, C.F. & Halpert, M.S. (1987) Global and regional scale precipitation patterns associated with the El Niño/southern oscillation. *Monthly Weather Review*, 115, 1606–1626. Available from: https://doi.org/10.1175/1520-0493(1987)115%3C1606:GARSPP%3E2.0.CO;2
Rosenblum, M., Pikovsky, A. & Kurths, J. (2001) Phase synchronization: from theory to data analysis. In: *Handbook of biological physics*, Vol. 9, North-Holland: Elsevier Science B.V, pp. 279–321.
Salas, H.D. (2020) *Synchronization and interdependence between the cycles of Colombia's hydroclimatology and El Niño-southern oscillation*. Ph.D. thesis. Colombia: Universidad Nacional de Colombia. Available from: https://repositorio.unal.edu.co/handle/unal/78420
Salas, H.D., Poveda, G., Mesa, O.J. & Marwan, N. (2020) Generalized synchronization between enso and hydrological variables in Colombia: a recurrence quantification approach. *Frontiers in Applied Mathematics and Statistics*, 6, 1–20.
Salas, H.D., Valencia, J., Builes-Jaramillo, A. & Jaramillo, A. (2022) Synoptic time scale variability in precipitation and streamflows for river basins over northern South America. *Hydrology*, 9, 59. Available from: https://www.mdpi.com/2306-5338/9/4/59
Sanabria, J., Bourrel, L., Dewitte, B., Frappart, F., Rau, P., Solis, O. et al. (2018) Rainfall along the coast of Peru during strong el niño events. *International Journal of Climatology*, 38, 1737–1747.
Sarachik, E.S. & Cane, M.A. (2010) *The El Niño–southern oscillation phenomenon*. New York: Cambridge University Press.
Satyamurty, P., Costa, C.P.W.D., Manzi, A.O. & Candido, L.A. (2013) A quick look at the 2012 record flood in the amazon basin. *Geophysical Research Letters*, 40, 1396–1401.
Schiff, S.J., So, P., Chang, T., Burke, R.E. & Sauer, T. (1996) Detecting dynamical interdependence and generalized synchrony through mutual prediction in a neural ensemble. *Physical Review E*, 54, 6708–6724.
Segura, H., Junquas, C., Espinoza, J.C., Vuille, M., Jauregui, Y.R., Rabatel, A. et al. (2019) New insights into the rainfall variability in the tropical andes on seasonal and interannual time scales. *Climate Dynamics*, 53, 405–426.
Shimizu, M.H., Ambrizzi, T. & Liebmann, B. (2017) Extreme precipitation events and their relationship with ENSO and MJO phases over northern South America. *International Journal of Climatology*, 37, 2977–2989. Available from: https://doi.org/10.1002/joc.4893
Singh, M., Krishnan, R., Goswami, B., Choudhury, A.D., Swapna, P., Vellore, R. et al. (2020) Fingerprint of volcanic forcing on the enso–indian monsoon coupling. *Science Advances*, 6, 1–12.
Stein, K., Timmermann, A. & Schneider, N. (2011) Phase synchronization of the el niño-southern oscillation with the annual cycle. *Physical Review Letters*, 107, 128501.
Stein, K., Timmermann, A., Schneider, N., Jin, F.-F. & Stuecker, M.F. (2014) Enso seasonal synchronization theory. *Journal of Climate*, 27, 5285–5310.
Strogatz, S.H. (2003) *Sync: the emerging science of spontaneous order*. New York: Hyperion.
Sulca, J. (2021) Evidence of nonlinear walker circulation feedbacks on extreme el niño pacific diversity: observations and cmip5 models. *International Journal of Climatology*, 41, 2934–2961. Available from: https://doi.org/10.1002/joc.6998
Sulca, J., Takahashi, K., Espinoza, J.C., Tacza, J., Zubieta, R., Mosquera, K. et al. (2024) A multiple linear regression model for the prediction of summer rainfall in the northwestern peruvian amazon using large-scale indices. *Climate Dynamics*, 1–21.
Sulca, J., Takahashi, K., Espinoza, J.C., Vuille, M. & Lavado-Casimiro, W. (2018) Impacts of different ENSO flavors and tropical Pacific convection variability (ITCZ, SPCZ) on austral summer rainfall in South America, with a focus on Peru. *International Journal of Climatology*, 38, 420–435.

Sullivan, A., Luo, J.-J., Hirst, A.C., Bi, D., Cai, W. & He, J. (2016) Robust contribution of decadal anomalies to the frequency of central-pacific el niño. *Scientific Reports*, 6, 38540.

Takahashi, K. & Martínez, A.G. (2019) The very strong coastal el niño in 1925 in the far-eastern pacific. *Climate Dynamics*, 52, 7389–7415.

Takahashi, K., Montecinos, A., Goubanova, K. & Dewitte, B. (2011) ENSO regimes: reinterpreting the canonical and Modoki El Niño. *Geophysical Research Letters*, 38, 1–5.

Tedeschi, R.G. & Collins, M. (2016) The influence of enso on south american precipitation during austral summer and autumn in observations and models. *International Journal of Climatology*, 36, 618–635.

Terray, P., Delecluse, P., Labattu, S. & Terray, L. (2003) Sea surface temperature associations with the late Indian summer monsoon. *Climate Dynamics*, 21, 593–618.

Timmermann, A., An, S.-I., Kug, J.-S., Jin, F.-F., Cai, W., Capotondi, A. et al. (2018) El Niño-southern oscillation complexity. *Nature*, 559, 535–545. Available from: http://www.nature.com/articles/s41586-018-0252-6

von Storch, H., Bürger, G., Schnur, R. & von Storch, J.-S. (1995) Principal oscillation patterns: a review. *Journal of Climate*, 8, 377–400.

Wang, C. (2007) Variability of the caribbean low-level jet and its relations to climate. *Climate Dynamics*, 29, 411–422.

Wang, C., Deser, C., Yu, J.-Y., DiNezio, P. & Clement, A. (2017) El Niño and southern oscillation (ENSO): a review. *Coral Reefs of the Eastern Tropical Pacific*, 8, 85–106.

Wang, C. & Picaut, J. (2004) Understanding ENSO physics - A review. In: Wang, C., Xie, S.-P., & Carton, J. A. (Eds.) *Earth's climate: The ocean-atmosphere interaction, Geophysical Monograph Series*, Vol. 147, Washington, D. C: AGU, pp. 21–48.

Wang, X.-Y., Zhu, J., Chang, C.-H., Johnson, N.C., Liu, H., Li, Y. et al. (2021) Underestimated responses of walker circulation to enso-related sst anomaly in atmospheric and coupled models. *Geoscience Letters*, 8, 17.

Waylen, P. & Poveda, G. (2002) El niño-southern oscillation and aspects of western south american hydro-climatology. *Hydrological Processes*, 16, 1247–1260.

Wiedermann, M., Siegmund, J.F., Donges, J.F. & Donner, R.V. (2021) Differential imprints of distinct ENSO flavors in global patterns of very low and high seasonal precipitation. *Frontiers in Climate*, 3, 1–14.

Wu, Z. & Huang, N.E. (2009) Ensemble empirical mode decomposition: a noise-assited data analysis method. *Advances in Adaptive Data Analysis*, 01, 1–41. Available from: https://doi.org/10.1142/S1793536909000047

Wu, Z., Schneider, E.K., Kirtman, B.P., Sarachik, E.S., Huang, N.E. & Tucker, C.J. (2008) The modulated annual cycle: an alternative reference frame for climate anomalies. *Climate Dynamics*, 31, 823–841. Available from: https://doi.org/10.1007/s00382-008-0437-z

Xie, P. & Arkin, P.A. (1997) Global precipitation: a 17-year monthly analysis based on gauge observations, satellite estimates, and numerical model outputs. *Bulletin of the American Meteorological Society*, 78, 2539–2558. Available from: https://doi.org/10.1175/1520-0477(1997)078%3C2539:GPAYMA%3E2.0.CO;2

Xie, Z., Duan, A. & Tian, Q. (2017) Weighted composite analysis and its application: an example using ENSO and geopotential height. *Atmospheric Science Letters*, 18, 435–440.

Yang, X., Bao, Y., Song, Z., Shu, Q., Song, Y., Wang, X. et al. (2023) Key to enso phase-locking simulation: effects of sea surface temperature diurnal amplitude. *npj Climate and Atmospheric Science*, 6, 159.

Yepes, J., Poveda, G., Mejía, J.F., Moreno, L. & Rueda, C. (2019) Choco-jex: a research experiment focused on the chocó low-level jet over the far eastern pacific and western Colombia. *Bulletin of the American Meteorological Society*, 100, 779–796.

Yoon, J.-H. & Zeng, N. (2010) An atlantic influence on amazon rainfall. *Climate Dynamics*, 34, 249–264.

Yun, K.-S., Timmermann, A. & Stuecker, M.F. (2021) Synchronized spatial shifts of hadley and walker circulations. *Earth System Dynamics*, 12, 121–132.

Zheng, F., Fang, X.H., Yu, J.Y. & Zhu, J. (2014) Asymmetry of the Bjerknes positive feedback between the two types of El Niño. *Geophysical Research Letters*, 41, 7651–7657.

SUPPORTING INFORMATION

Additional supporting information can be found online in the Supporting Information section at the end of this article.

How to cite this article: Salas, H. D., Builes-Jaramillo, A., Boers, N., Poveda, G., Mesa, Ó. J., & Kurths, J. (2024). Precipitation over northern South America and the far-eastern Pacific during ENSO: Phase synchronization at inter-annual time scales. *International Journal of Climatology*, 1–18. https://doi.org/10.1002/joc.8443

No.	NOMBRE	ISSN	CATEGORIA	VIGENCIA	LISTA_SIR
11303	MILITARY PSYCHOLOGY	0899-5605; 1532-7876	A2	Enero 2024 - Junio 2024	PsycINFO; Social Science Citation Index - SSCI; Scimago Journal Rank - SJR; Journal Citation Reports - JCR
11304	CRITICAL CARE NURSING CLINICS OF NORTH AMERICA	0899-5885; 1558-3481	A2	Enero 2024 - Junio 2024	Science Citation Index - SCI; Social Science Citation Index - SSCI; Scimago Journal Rank - SJR; Journal Citation Reports - JCR
11305	CLINICAL IMAGING	0899-7071; 1873-4499	A2	Enero 2024 - Junio 2024	Science Citation Index - SCI; Scimago Journal Rank - SJR; Journal Citation Reports - JCR
11306	JOURNAL OF AQUATIC ANIMAL HEALTH	0899-7659; 1548-8667	A2	Enero 2024 - Junio 2024	Science Citation Index - SCI; Scimago Journal Rank - SJR; Journal Citation Reports - JCR
11307	INTERNATIONAL JOURNAL OF CLIMATOLOGY	0899-8418; 1097-0088	A2	Enero 2024 - Junio 2024	Science Citation Index - SCI; Scimago Journal Rank - SJR; Journal Citation Reports - JCR
11308	PEDIATRIC EXERCISE SCIENCE	0899-8493; 1543-2920	A2	Enero 2024 - Junio 2024	Science Citation Index - SCI; Scimago Journal Rank - SJR; Journal Citation Reports - JCR
11309	NUTRITION	0899-9007; 1873-1244	A2	Enero 2024 - Junio 2024	Science Citation Index - SCI; Scimago Journal Rank - SJR; Journal Citation Reports - JCR
11310	INTERNATIONAL JOURNAL OF IMAGING SYSTEMS AND TECHNOLOGY	0899-9457; 1098-1098	A2	Enero 2024 - Junio 2024	Science Citation Index - SCI; Scimago Journal Rank - SJR; Journal Citation Reports - JCR
11311	AIDS EDUCATION AND PREVENTION	0899-9546; 1943-2755	A2	Enero 2024 - Junio 2024	PsycINFO; Social Science Citation Index - SSCI; Scimago Journal Rank - SJR; Journal Citation Reports - JCR
11312	CLINICAL TRANSPLANTATION	0902-0063; 1399-0012	A2	Enero 2024 - Junio 2024	Science Citation Index - SCI; Scimago Journal Rank - SJR; Journal Citation Reports - JCR
11313	APMIS	0903-4641; 1600-0463	A2	Enero 2024 - Junio 2024	Science Citation Index - SCI; Scimago Journal Rank - SJR; Journal Citation Reports - JCR
11314	HERMES	0904-1699; 1903-1785	A2	Enero 2024 - Junio 2024	Scimago Journal Rank - SJR